water

MDPI

Article

Using Tabu Search Adjusted with Urban Sewer Flood Simulation to Improve Pluvial Flood Warning via Rainfall Thresholds

Hao-Yu Liao [1], Tsung-Yi Pan [2], Hsiang-Kuan Chang [2], Chi-Tai Hsieh [2], Jihn-Sung Lai [1,2,3,4,*], Yih-Chi Tan [1,2,3] and Ming-Daw Su [3]

1 Research Center of Climate Change and Sustainable Development, National Taiwan University, Taipei 10617, Taiwan; hyu14116@gmail.com (H.-Y.L.); yctan95@126.com (Y.-C.T.)
2 Center for Weather Climate and Disaster Research, National Taiwan University, Taipei 10617, Taiwan; tsungyi.pan@gmail.com (T.-Y.P.); akuanchang@gmail.com (H.-K.C.); chitai@mail2000.com.tw (C.-T.H.)
3 Department of Bioenvironmental Systems Engineering, National Taiwan University, Taipei 10617, Taiwan; sumd@ntu.edu.tw
4 Hydrotech Research Institute, National Taiwan University, Taipei 10617, Taiwan
* Correspondence: jslai525@ntu.edu.tw; Tel.: +886-2-33662617

Received: 15 January 2019; Accepted: 12 February 2019; Published: 18 February 2019

Abstract: Pluvial floods are the most frequent natural hazard impacting urban cities because of extreme rainfall intensity within short duration. Owing to the complex interaction between rainfall, drainage systems and overland flow, pluvial flood warning poses a challenge for many metropolises. Although physical-based flood inundation models could identify inundated locations, hydrodynamic modeling is limited in terms of computational costs and sophisticated calibration. Thus, herein, a quick pluvial flood warning system using rainfall thresholds for central Taipei is developed. A tabu search algorithm is implemented with hydrological-analysis-based initial boundary conditions to optimize rainfall thresholds. Furthermore, a cross test is adopted to evaluate the effect of each rainfall event on rainfall threshold optimization. Urban sewer flood is simulated via hydrodynamic modeling with calibration using crowdsourced data. The locations and time of occurrence of pluvial floods can be obtained to increase the quality of observed data that dominate the accuracy of pluvial flood warning when using rainfall thresholds. The optimization process is a tabu search based on flood reports and observed data for six flood-prone districts in central Taipei. The results show that optimum rainfall thresholds can be efficiently determined through tabu search and the accuracy of the issued flood warnings can be significantly improved.

Keywords: tabu search; urban sewer; pluvial flood; rainfall threshold; crowdsourced data; flood warning

1. Introduction

Pluvial flooding can be a serious problem in cities with a densely populated urban area. It is typically caused by intensive rainfall and drainage capacity exceedance can result in severe impacts on the drainage systems in cities. Torrential rainfalls have caused serious flooding damages in the Taipei metropolitan area in recent decades, often induced by typhoon or rainstorm events [1–5]. For disaster preparedness and mitigation, providing timely and effective information to individuals exposed to a hazard is an important task to reduce their risk and avoid flood damage. To deliver effective flood warning information for the general public, the rainfall threshold approach is commonly used. For a given period of time, rainfall threshold is defined as a cumulative rainfall depth that can generate the critical runoff to cause flood disasters. Thus, the value of the rainfall threshold is used as a preliminary

reference to issue flood warnings, in lieu of more sophisticated hydrodynamic simulations [6,7]. Complex numerical models can be adopted to calculate pluvial flooding for detailed hydrodynamic phenomena in an urban sewer drainage system. However, numerical simulations for pluvial flood forecasting are rather computationally costly. In contrast, the rainfall threshold approach is relatively simple and effective and it has been adopted in several applications of disaster operations such as providing flood, landslide or debris flow warnings [8–10].

Researchers have developed various flood inundation models for providing pluvial flood warning information in urban areas [11–13]. Several studies have established rainfall thresholds for townships with high levels of urbanization and dense population in Taiwan [1,7,14]. Wu and Wang (2009) [1] used cumulative rainfalls and local historical flood records to empirically determine rainfall thresholds; however, the study lacked statistical analysis, instead relying on qualitative judgments to determine the thresholds on the basis of flood observation information. Jang (2015) [7] developed multiple rainfall thresholds for urban flood warnings. The multiple values of rainfall threshold at a specific township were updated according to the cumulative rainfall records of the latest flood event. In the updating process, the rainfall threshold was raised when the event encountered a non-flooding situation with rainfall larger than the previous one and vice versa. However, it is inconvenient that the proposed multiple rainfall thresholds need to be updated at least three times a year. Yang et al. (2016) [14] integrated rainfall thresholds and ensemble precipitation forecasting to issue flood warnings and estimate urban inundation risk. Collectively, these studies show that the rainfall threshold approach is able to activate flood warnings for pluvial flooding.

The rainfall threshold approach has proven to be useful in identifying flash flood events in many cases [15,16]. Whereas the rainfall threshold approach should not be considered as a replacement for a hydrodynamic model because of its simplicity, a rainfall threshold approach to develop a flood warning system can be an immediately useful tool for a variety of decision makers interested in early warnings for flash floods [17]. Several previous studies have applied rainfall thresholds to evaluate urban inundation risk [7,18]. The Water Resource Agency (WRA) of Taiwan has established rainfall thresholds for over 400 districts and townships in Taiwan. The procedures used to determine the WRA rainfall thresholds (WRTs) are illustrated in Figure 1 [1]. First of all, the WRA collects historical flood records, including typhoons, heavy rains and other rainfall events that cause flooding, before selecting rain gauges that are in proximity to the flooding locations and then evaluates the relationship between 1-, 3-, 6-, 12- and 24-h cumulative rainfalls and flood occurrence. The setup of the initial rainfall thresholds can be decided by adjusting the cumulative rainfalls. Finally, rainfall thresholds are modified through local drainage capacity, rainfall return period and other local infrastructures before judgment by professional experts. However, the WRTs need more adjustment because false alarms may happen frequently.

Several algorithms such as simulated annealing, genetic algorithm and tabu search (TS) are often applied to deal with optimization problems. Among the algorithms, TS has provided better solutions than the others [19–22]. Thus, the study adopts TS to solve optimization problems of rainfall thresholds. TS was first introduced in 1986 [23–26]. Several hydrology-related issues have been using this superior algorithm to solve optimization problems, such as groundwater [27–29], reservoir operation [30] and river flow [31]. The advantages of TS are that it can efficiently deal with highly nonlinear problems [32], allows solutions to move temporarily to worse solutions that might be routed to global optimal solution [33] and has few parameters [28]. In order to improve the flood warnings via rainfall thresholds, the optimal rainfall thresholds (ORTs) are determined via TS. In addition, the simulated results from hydrodynamic modeling will be applied to improve the quality of inputs for TS.

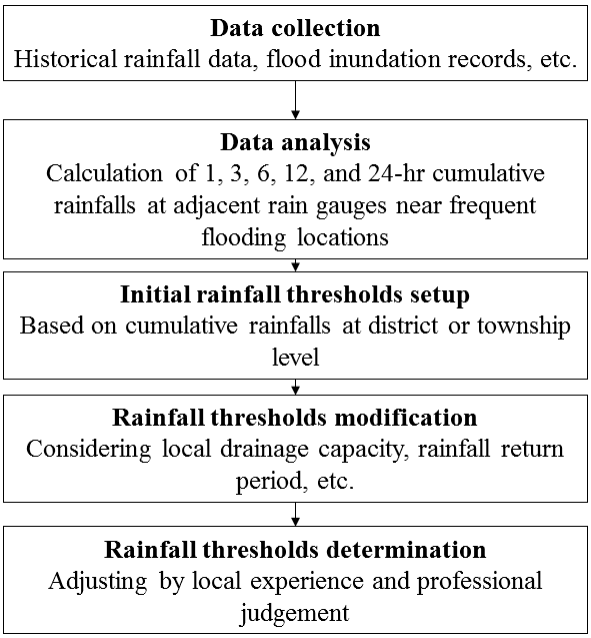

Figure 1. The procedures for determining Water Resource Agency rainfall thresholds (WRTs).

Due to increasingly attractive simulation solutions, hydrodynamic numerical modeling techniques with large computing capabilities in recent years have become popular. Hydrodynamic numerical models include the SOBEK model [34], FLO-2D [35] and 2D-DOFM [36]. SOBEK is an integrated modeling framework for river, estuary and storm sewer water systems, which is capable of simulating hydrodynamics of flood inundation phenomena. The model can estimate pluvial flooding coupled with a hydrological model for flood retardation and damage mitigation. For determining the start time of manhole overflow in inundation areas, urban sewer flood simulation performed by SOBEK model is adopted to this study. Several studies have used the SOBEK model to deal with hydrodynamics issues [37–42]. The water level variations of storm water systems and flood inundation extents are simulated by the SOBEK model, which is calibrated and validated with observed data.

Recently, exploiting crowdsourced natural disaster data has garnered a great deal of attention. There is often a lack of sufficient monitoring sensors or measuring equipment and information describing the field conditions and consequences is rarely available in real time. However, due to the availability of mobile devices, observation information contributed by individuals via social media is conveniently valuable to document flood events directly. The social media content based on eyewitness observations can be retrieved by searching and sorting keywords such as flooding location, time and water depth [43,44]. This information source should be explored and implemented in a more effective way which improves the information basis for disaster assessment and response [45,46]. Therefore, the crowdsourced observation data related to flooding will be utilized for model calibration in this study.

The study proposes a pluvial flood warning model using TS to find ORTs and adjusted ORTs via a hydrodynamic modeling that provides the start time of floods. The first step is to define rainfall events via inter-event times and cumulative rainfall criteria. Then, the start time of floods is determined by the hydrodynamic modeling based on completely divided rainfall events. Finally, ORTs, cross test ORTs and adjusted ORTs are computed via TS. The results show that ORTs based on TS can be used in urban flood warnings and the adjusted ORTs can yield even more warning time.

2. Study Area and Data

2.1. Central Area of Taipei

The study area located in the central area of Taipei is densely populated and highly developed as the political and economic center of Taiwan. As shown in Figure 2, it is surrounded by the Tamsui River on the west, the Xindian River on the south, the Keelung River on the north and hills on the southeast and east. This study area has six flood-prone districts protected by the high raised levees along the rivers and dozens of pumping stations, all of which were built for flood control. Because the study area is protected by 200-year return-period-designed flood levees, the major type of flooding is pluvial, which occurs when a heavy rain exceeds the discharge capacity of the urban sewer systems.

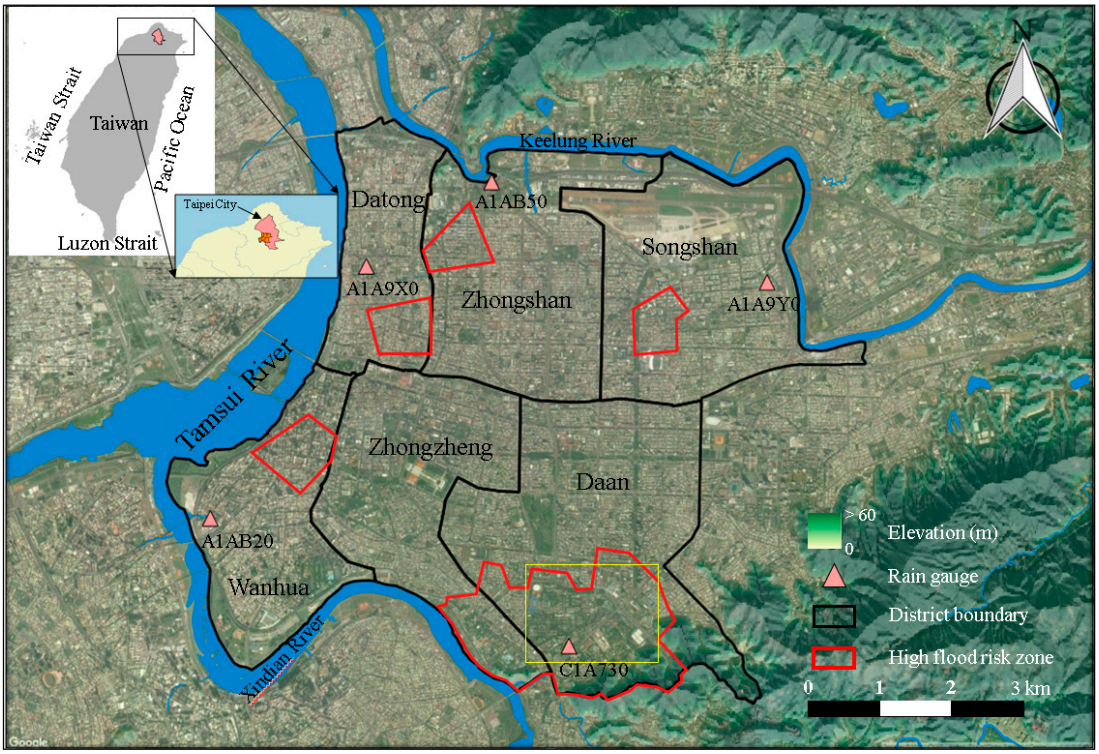

Figure 2. Flood warning districts and rain gauge locations in central Taipei.

Five rain gauges are used to issue flood warnings in central Taipei and the location, start time and number of rainfall events are shown in Figure 2 and Table 1. The number of rainfall events ranges from 686 to 957 collected from 2012 to 2017. Each rain gauge can trigger an alert to the inundation area.

Table 1. The rain gauges in central Taipei and WRTs of the five rain gauges for flood warnings to six districts within central Taipei.

Name	ID	Warning District	WRA Rainfall Threshold of Each Duration (mm)			No. of Rainfall Events (2012–2017)
			1 h	3 h	6 h	
Taiping	A1A9X0	Datong	60	110	160	686
Jianguo	A1AB50	Zhongshan	60	100	150	704
Minsheng	A1A9Y0	Songshan	60	110	170	730
Shuangyuan	A1AB20	Wanhua	60	120	150	713
Gongguan	C1A730	Zhongzheng	60	120	150	957
Gongguan	C1A730	Daan	60	100	140	957

2.2. WRA Pluvial Flood Warning

The WRA has established 754 sets of rainfall thresholds based on 500 rain gauges, including those in central Taipei, for 368 districts in Taiwan. Each set is composed of 1-, 3- and 6-h rainfall thresholds

that are determined from flood records. In this study, six sets of rainfall thresholds based on five rain gauges are shown in Table 1. According to Table 1, the 1-h rainfall thresholds of all rain gauges are the same, whereas the 3-h and 6-h rainfall thresholds vary from 100 mm to 120 mm and from 140 mm to 170 mm, respectively. These values correspond to the status of the drainage systems in Taipei, for which the design capacity is 78.8 mm/hr. In order to improve the accuracy of pluvial flood warning, this study refers to FFG [47] to select the 1-, 3-, 6-, 12- and 24-h rainfall thresholds herein.

2.3. Flood Events

From 2012 to 2017, 23 flood events including 14 heavy rains and nine typhoons caused inundation in six districts of central Taipei as shown in Table 2. According to Table 2, most of the heavy rains were stationary fronts, called Mei-yu fronts, which occurred during May and June and five of the heavy rains were thundershowers, which tend to produce a lot of rain within a very brief timeframe. Also, nine typhoons were selected to optimize the rainfall thresholds. These typhoons, including Typhoon Saola, Typhoon Trami, Typhoon Soudelor, Typhon Dujuan and Typhoon Megi, caused over 200 mm of rainfall in 24 h as shown in Figure 3. According to Figure 3, the 3-, 6-, 12- and 24-h cumulative rainfalls of thundershower events, such as Heavy rain 0814 and Heavy rain 0822 in 2013 and Heavy rain 0723, Heavy rain 0818 and Heavy rain 0827 in 2015, are always similar because thundershowers produce a large amount of rain very quickly. The long-duration rainfall events always occur in typhoons or Mei-yu fronts. As a result, the cumulative rainfalls for 1-, 3-, 6-, 12- and 24-h durations at each Mei-yu front and typhoon can be quite different. Four events, including Heavy rain 0519 in 2014, Heavy rain 0723 in 2015 and Typhoon Soudelor in 2015 and Heavy rain 0602 in 2017, were selected to conduct urban flood simulations that determine the start time of floods to adjust rainfall thresholds.

Table 2. Historical flood events for central Taipei from 2012 to 2018.

No.	Event	Date	Warning District					
			Datong	Zhongshan	Songshan	Wanhua	Zhongzheng	Daan
E01	Heavy rain 0502	2012/05/02	0	0	0	0	1	0
E02	Heavy rain 0610	2012/06/10	0	1	1	1	0	1
T01	Typhoon Saola	2012/08/02	0	1	0	0	1	1
T02	Typhoon Soulik	2013/07/11	0	0	1	0	0	1
E03	Heavy rain 0814	2013/08/14	1	1	0	1	0	0
T03	Typhoon Trami	2013/08/20	0	1	1	1	0	1
E04	Heavy rain 0822	2013/08/22	1	0	1	1	1	1
T04	Typhoon Kong-rey	2013/08/28	0	1	0	1	1	0
T05	Typhoon Fitow	2013/10/06	1	0	0	0	0	0
E05	Heavy rain 0515	2014/05/15	0	0	1	0	0	0
E06	Heavy rain 0519	2014/05/19	0	1	1	1	1	1
E07	Heavy rain 0605	2014/06/05	0	0	1	0	0	0
E08	Heavy rain 0614	2015/06/14	0	0	1	0	1	1
T06	Typhoon Chan-hom	2015/07/09	0	0	1	0	0	0
E09	Heavy rain 0723	2015/07/23	1	1	0	0	0	1
T07	Typhoon Soudelor	2015/08/07	1	1	1	1	1	1
E10	Heavy rain 0818	2015/08/18	1	0	0	0	0	1
E11	Heavy rain 0827	2015/08/27	0	1	0	0	1	0
T08	Typhoon Dujuan	2015/09/28	0	0	1	0	1	0
E12	Heavy rain 0617	2016/06/17	0	1	1	0	0	1
T09	Typhoon Megi	2016/09/25	0	1	0	0	0	1
E13	Heavy rain 0602	2017/06/02	1	1	1	1	1	1
E14	Heavy rain 0613	2017/06/13	0	1	0	0	0	0
E15	Heavy rain 0908	2018/09/08	1	1	1	1	1	1
	Total		8	14	14	9	11	14

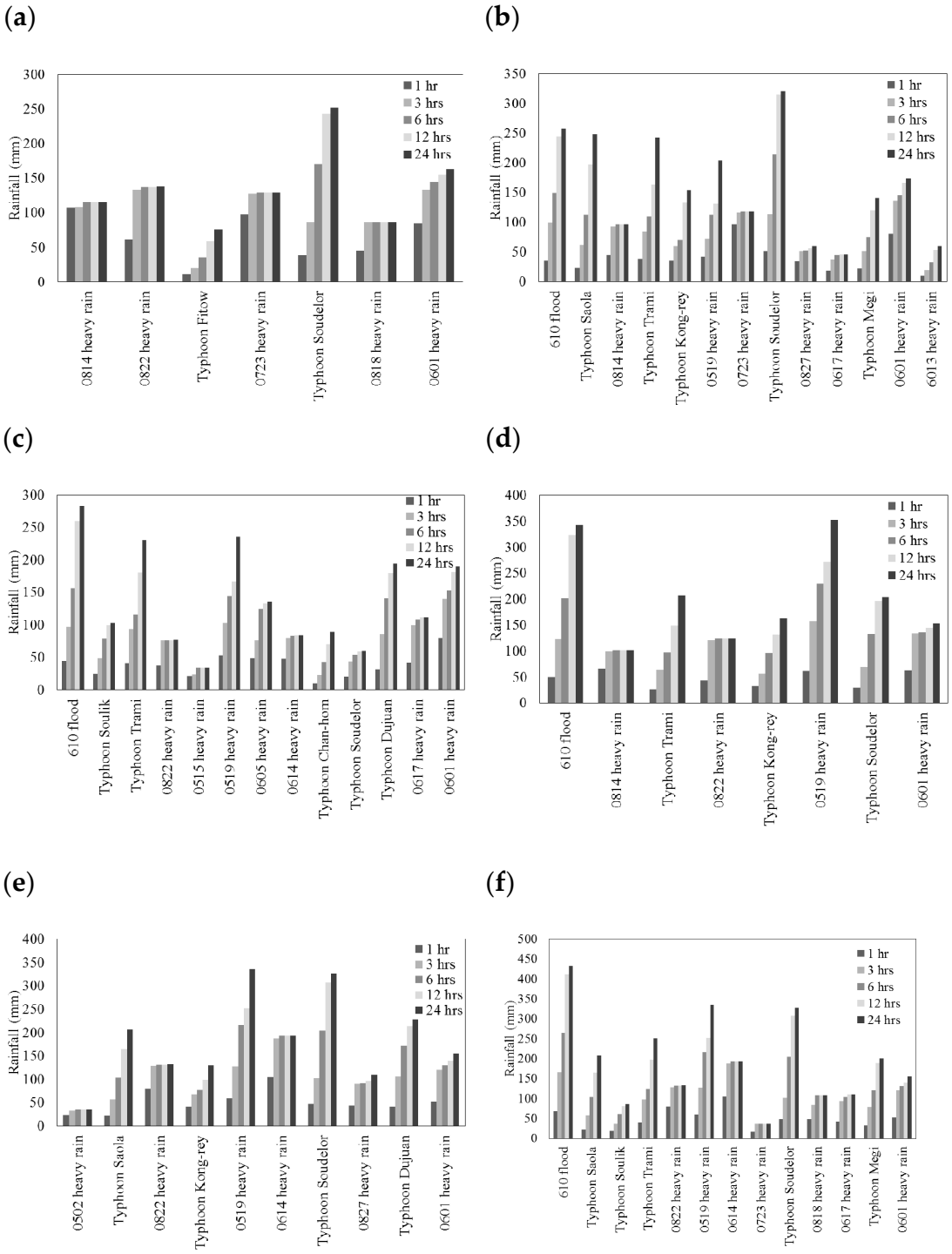

Figure 3. The maximum cumulative rainfalls for 1-, 3-, 6-, 12- and 24-h durations in six districts: (**a**) Datong; (**b**) Zhongshan; (**c**) Songshan; (**d**) Wanhua; (**e**) Zhongzheng; and (**f**) Daan.

3. Methodology

3.1. Urban Sewer Flood Simulation

3.1.1. Hydrodynamic Modeling

Overflow occurs when water is lost from the sewer conduit to the ground surface. When sewer water overflows to the ground surface, it runs as overland flow to cause flood inundation. In order to

understand the hydrodynamic phenomena, the overflow process and flood inundation in the study area were simulated by the SOBEK model. The model solves the Saint–Venant equations by integrating the one-dimensional (1D) sewer flow and the two-dimensional (2D) overland flow modeling with a rainfall-runoff calculation. The model is applied to simulate the variable flow velocities, water levels and inundation extents associated with flooding events in urban sewer systems. Since the study area consists of both rivers and sewer systems in Taipei, we divided the simulation domain into rivers, urban sewer areas and surface runoff catchments. In the rainfall-runoff calculation, the Soil Conservation Service curve number (CN) is adopted according to land use in the catchment areas and a rational formula is used in the urban sewer areas. Roughness (n) along the rivers and sewer systems is calculated using the Manning formula. The linkage of the integrated model includes the following: (1) for the 1D sewer flow model, the hydrographs of overflow rate are calculated at each manhole when the surface runoff exceeds the design capacity of the sewer system; (2) for the 2D overland flow model, overland flow is calculated to obtain water depth and velocity by using the overflow hydrographs as sources. Historical rainfall and flooding records are used in calibrating some parameters such as the CN and Manning roughness.

3.1.2. Validation Using Crowdsourced Data

In situ observations of flooding locations and inundation depth by local people were reported through the Emergency Management Information Cloud (EMIC) system developed in 2015 that utilizes cloud computing technology and cross-agency disaster-related information for the support of decision making at the Central Emergency Operation Center, Taiwan. These reported data contain the location, time and water depth within the period of flooding. From the reported observations, the times during which manholes were under overflow conditions in flood inundation areas can be identified. Although only a limited amount of flood information data could be retrieved from the EMIC, the crowdsourced data will be useful for model validation.

High rainfall intensity during the Heavy rain 0602 (2017) and Heavy rain 0723 (2015) events caused pluvial flooding in central Taipei. The rainfall records of these two flood events shown in Figure 4; Figure 5 are used to calibrate the parameters in the SOBEK model. The model calibration process consisted of modifying the input parameters until the output from the model matched the observed data. By using digital elevation model data with a spatial resolution of 10 m $\times$ 10 m (grid size) in the simulation domains, at each grid, the simulated results of water depth greater than 0.1 m was considered as flooding. The simulated overflow hydrographs of discharge and water level at the manholes in the sewer system were obtained. In Figure 4a, the water level hydrograph is plotted for Heavy rain 0602 (2017) event. From the limited flood information retrieved from EMIC, four reported flooding observations at various times in Datong district are marked and plotted in Figure 4a. As shown in Figure 4a, at 12:08, the first report of flooding is close to the peak time of the water level hydrograph and the rest of the reported data are around the period of time when the water was overflowing from the sewer conduit to the ground surface. A comparison of the observed and simulated overflow times reveals that the pluvial flooding situations can be properly modeled by the SOBEK model, as plotted in Figures 4 and 5. The parameter values of CN and n should affect the simulated values for sewer system depth and velocity and flood inundation depth and extent under overflow situations. From the model calibration for optimal values, the CN and n parameters range from 39 to 98 and from 0.015 to 0.035, respectively, which are similar to those of previous studies [41,42].

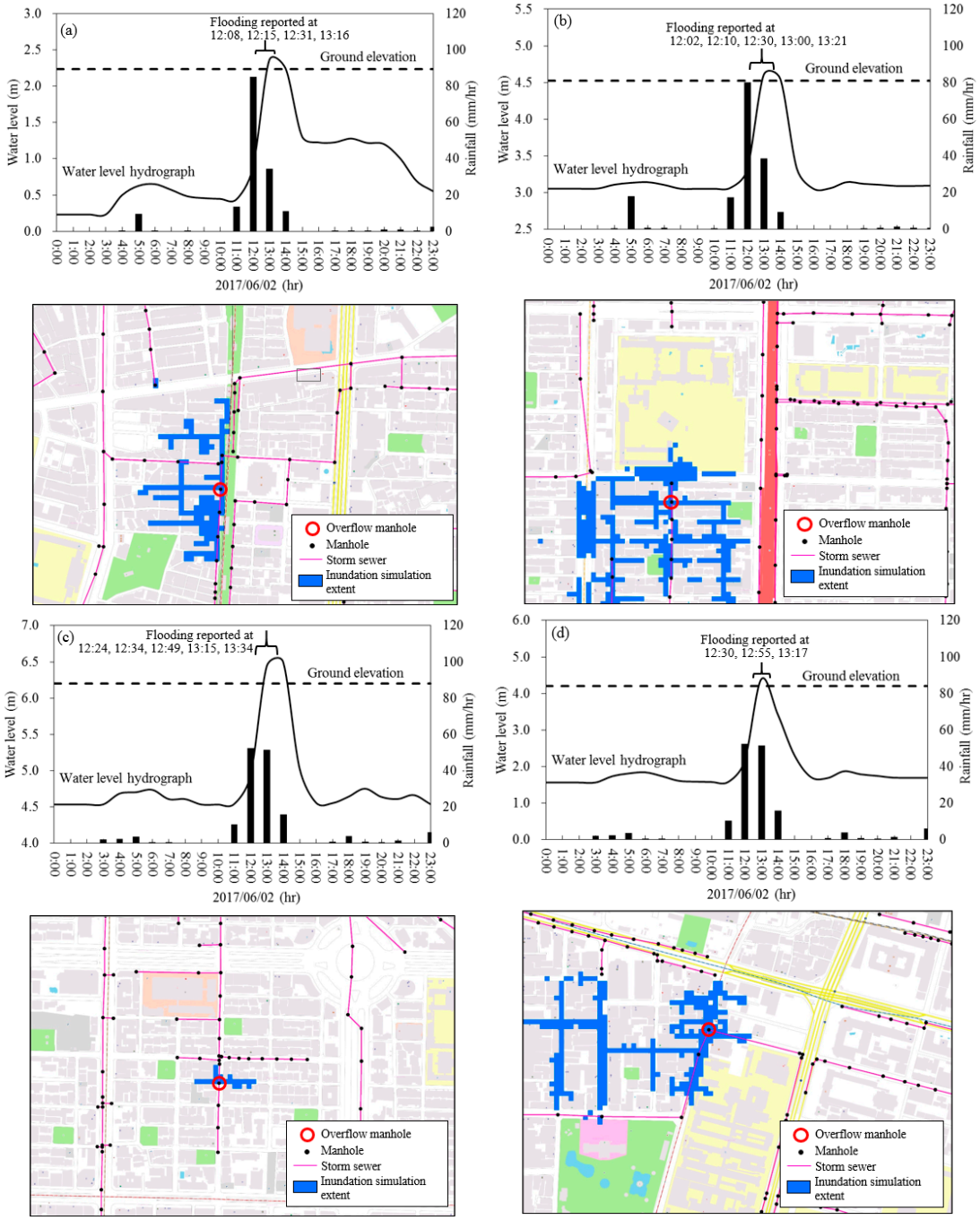

Figure 4. Simulated flood inundation depth and extent during Heavy rain 0602 (2017) in (**a**) Datong district, (**b**) Zhongshan district, (**c**) Daan district and (**d**) Zhongzheng district.

In 2018, the social media analysis (SMA) system was developed by the program on Applying Science and Technology for Disaster Reduction which is sponsored by the Taiwan Ministry of Science and Technology. In the resent study, the system was employed to retrieve disaster-related information from various crowdsourced data Internet platforms such as news media and Internet forums. Individuals may contribute information which cannot be captured by sensors if the sensors are not available. Although these reported data might not be accurate enough, they are still practically applicable to provide, with photos or videos, approximate data regarding the location and time of flooding, overflow situations and so forth. By comparison with the flood information provided by the EMIC, these SMA data should also be helpful for model validation. In the Heavy rain 0908 (2018) event,

high rainfall intensity also caused pluvial flooding in central Taipei. The crowdsourced data were retrieved from EMIC and SMA every 10 min, in terms of social media post volume (number of posts) related to EMIC report, news media and Internet forums. Using the rainfall recorders for the Heavy rain 0908 (2018) event as input, the simulated water level hydrograph results are plotted in Figure 6 on Keelung Road in Daan district. As shown in Figure 6a, the social media post volume reached the highest when the water level was above the ground surface. When water level retreated, the social media post volume dropped simultaneously and the rainfall gradually eased. Several photos with their corresponding locations obtained from SMA are shown in Figure 6b. From the above analysis, the flooding simulation analysis is determined to be consistent with reality.

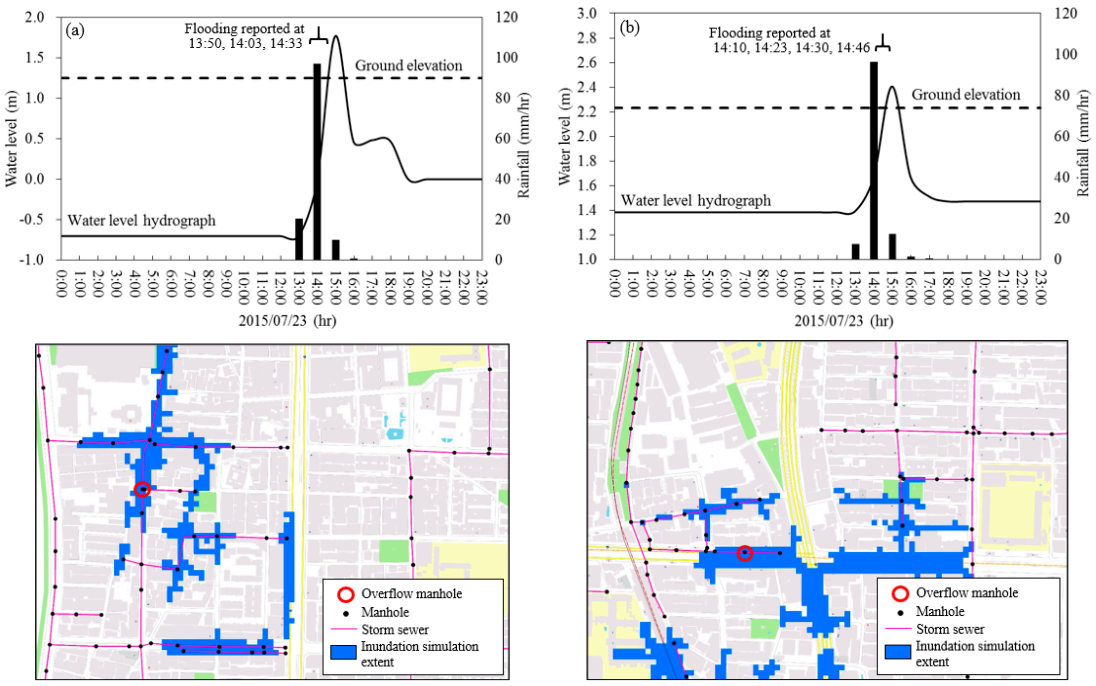

Figure 5. Simulated flood inundation depth and extent during Heavy rain 0723 (2015) in (**a**) Datong district and (**b**) Zhongshan district.

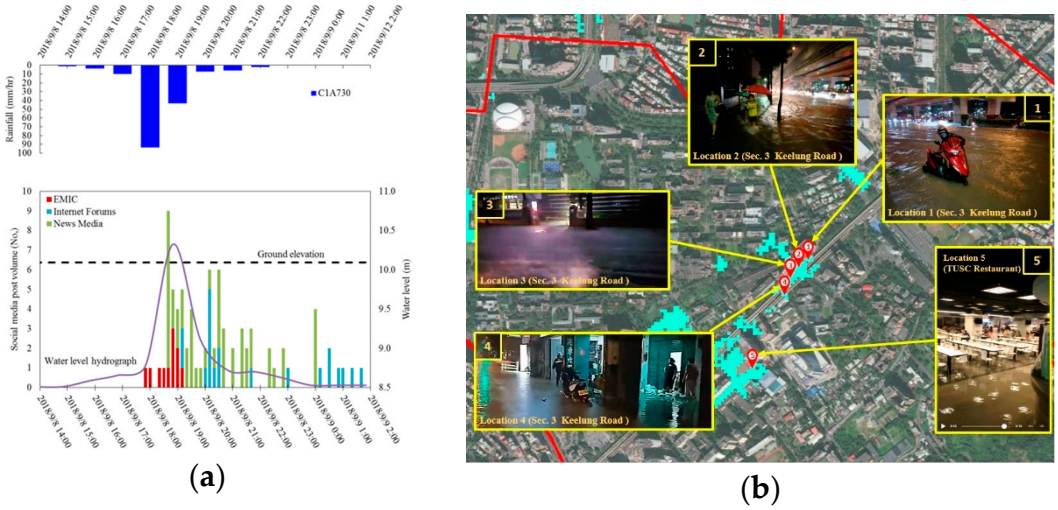

(**a**) (**b**)

Figure 6. A comparison of simulation results with crowdsourced data for Heavy rain 0908 (2018) along Keelung Road: (**a**) rainfall, water level and social media post volume; and (**b**) crowdsourced data of flooding locations with photos captured in situ.

3.2. Definition of a Rainfall Event

3.2.1. Inter-Event Time

The rainfall events can be delimited by inter-event time (IET). Each rainfall event is located between two IETs, the periods without rains [48,49]. Conventionally, the beginning of a rainfall event is defined as when the hourly rainfall becomes greater than 0.5 mm and the end of a rainfall event is marked by 4 h that is continuously without rain [50] as shown in Figure 7.

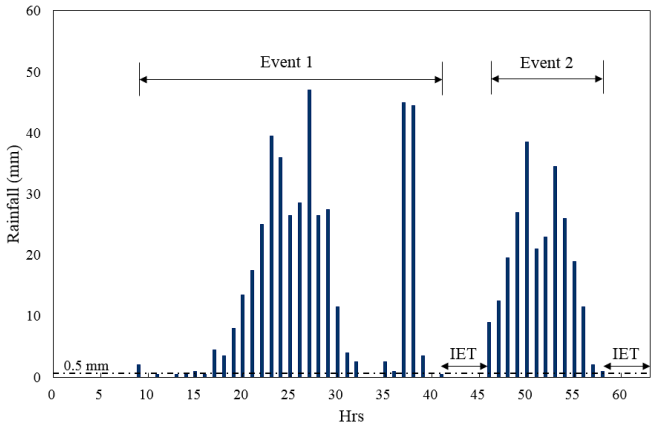

Figure 7. Rainfall events and inter-event time (IET).

The *j*th event of the *i*th rain gauge, $\text{Event}_{i,j}$, can be expressed in Equation (1) as:

$$\text{Event}_{i,j} = \left\{ r_{i,j,t_{begin}}, r_{i,j,t_{begin}+1}, \ldots, r_{i,j,t}, \ldots, r_{i,j,t_{end}-1}, r_{i,j,t_{end}} \middle| \begin{array}{l} r_{i,j,t_{begin}} \geq 0.5 \\ r_{i,j,t_{end+k}} = 0 \end{array} \right\}, \quad \text{for } i = 1, \ldots, 5 \text{ and } k = 1, \ldots, 4, \tag{1}$$

where $r_{i,j,t}$ is observed rainfall in the *j*th event of the *i*th rain gauge at time *t*.

3.2.2. Cumulative Rainfall Criteria

The relationship between rainfall and flooding has been discussed in several papers [51–54]. The occurrence probability of rain-related hazards like flooding is influenced by the amount of rainfall. The Central Weather Bureau (CWB) has analyzed the relationship between disasters and rainfall amount and it defines "heavy rain" as that having a rainfall intensity of at least 80 mm/24 h or 40 mm/h. The CWB also classifies heavy rainfall events into four categories, namely, heavy rain (80 mm/24 h or 40 mm/h), extremely heavy rain (200 mm/24 h or 100 mm/3 h), torrential rain (350 mm/24 h) and extremely torrential rain (500 mm/24 h). Therefore, the requirement of maximum cumulative rainfall should be satisfied if it meets the following criteria and the process could be denoted as:

$$MCR_{i,j,D} = \max_{t_{begin,j} \leq T \leq t_{end,j}-D+1} \left\{ \sum_{t=T}^{T+D-1} r_{i,j,t} \right\}, \text{ for } D = 1, 24. \tag{2}$$

$$CRC_{i,j} = \left\{ \begin{array}{l} 1 \ \ if \ MCR_{i,j,1} \geq 40 \ or \ MCR_{i,j,24} \geq 80 \\ 0 \end{array} \right\} \tag{3}$$

where *j* and *i* represent the event and rain gauge, respectively; *D* is the duration of the cumulative rainfall; and $CRC_{i,j}$ is the cumulative rainfall criteria result for the *j*th event at the *i*th rain gauge. If $CRC_{i,j}$ is equal to 0, this rainfall event at this rain gauge is not suitable for optimizing the rainfall thresholds. Thus, some unsuitable rainfall events can be removed by the procedure described in Equations (2) and (3).

3.3. Description of the Rainfall Threshold Model

3.3.1. Assessment Criteria

Several papers have discussed the relationship between flood warnings and flood events [7,17,55,56] as shown in Table 3.

Table 3. The relationship between warnings and floods.

Action Taken	Flood	No Flood
Warning	*Hit*	*False alarm*
No Warning	*Missed alarm*	*Correct rejection*

Table 3 lists all possible combinations in the relationship between flood warnings and flood events. *Hit* and *Correct rejection* represent the correct actions but the *Missed alarm* and *False alarm* represent the incorrect actions. The meaning of *Hit* is that the cumulative rainfalls exceed or reach rainfall thresholds and pluvial floods also occur; the meaning of *Missed alarm* is that pluvial floods occur without warning; *False alarm* means that the cumulative rainfalls reach the rainfall thresholds but pluvial floods do not occur; and *Correct rejection* means that cumulative rainfalls are lower than the rainfall thresholds and pluvial floods do not occur. Therefore, by applying Equations (2) and (3), each rainfall event can be classified into one of the four situations shown in Table 3 and this process can be expressed as:

$$HE_{i,j} = \left\{ \begin{array}{l} 1 \ if \ \left(\sum\limits_{D=1,\ 3,6,12,24} \ \sum\limits_{T=\ t_{begin,j}}^{t_{end,j}-D+1} \left\{ \begin{array}{l} 1 \ if \ \sum\limits_{t=T}^{T+D-1} r_{i,j,t} \geq RT_{i,D} \ and \ flood \\ 0 \end{array} \right\} \geq 1 \right) \\ 0 \end{array} \right\} \quad (4)$$

$$ME_{i,j} = \left\{ \begin{array}{l} 1 \ if \ \left(\sum\limits_{D=1,\ 3,6,12,24} \ \sum\limits_{T=\ t_{begin,j}}^{t_{end,j}-D+1} \left\{ \begin{array}{l} 1 \ if \ \sum\limits_{t=T}^{T+D-1} r_{i,j,t} < RT_{i,D} \ and \ flood \\ 0 \end{array} \right\} \geq 1 \right) \\ 0 \end{array} \right\} \quad (5)$$

$$FE_{i,j} = \left\{ \begin{array}{l} 1 \ if \ \left(\sum\limits_{D=1,\ 3,6,12,24} \ \sum\limits_{T=\ t_{begin,j}}^{t_{end,j}-D+1} \left\{ \begin{array}{l} 1 \ if \ \sum\limits_{t=T}^{T+D-1} r_{i,j,t} \geq RT_{i,D} \ and \ No \ flood \\ 0 \end{array} \right\} \geq 1 \right) \\ 0 \end{array} \right\} \quad (6)$$

$$CE_{i,j} = \left\{ \begin{array}{l} 1 \ if \ \left(\sum\limits_{D=1,\ 3,6,12,24} \ \sum\limits_{T=\ t_{begin,j}}^{t_{end,j}-D+1} \left\{ \begin{array}{l} 1 \ if \ \sum\limits_{t=T}^{T+D-1} r_{i,j,t} < RT_{i,D} \ and \ No \ flood \\ 0 \end{array} \right\} \geq 1 \right) \\ 0 \end{array} \right\} \quad (7)$$

where $HE_{i,j}$, $ME_{i,j}$, $FE_{i,j}$ and $CE_{i,j}$ mean that the rainfall events belong to *Hit*, *Missed alarm*, *False alarm* and *Correct rejection*, respectively and $RT_{i,D}$ is the rainfall threshold of the ith rain gauge with duration of D. The duration of D can be 1 h, 3 h, 6 h, 12 h or 24 h. With Equation (4), the event is classified into $HE_{i,j}$ when one of rainfall thresholds is met or exceeded. This study will focus on the occurrence frequency of $HE_{i,j}$ because this is the situation in which the residents have enough time for preparation and evacuation. The situation of $ME_{i,j}$ is the most dangerous because pluvial flooding occurs without any issued warnings. The situation of $FE_{i,j}$ reduces warning reliability. According to Equation (4) through Equation (7), the ORTs are based on three criteria as follows:

$$\text{CSI} = \frac{\sum_{i=1}^{n} HE_{i,j}}{\sum_{i=1}^{n} HE_{i,j} + \sum_{i=1}^{n} ME_{i,j} + \sum_{i=1}^{n} FE_{i,j}} \quad (8)$$

$$\text{POD} = \frac{\sum_{i=1}^{n} HE_{i,j}}{\sum_{i=1}^{n} HE_{i,j} + \sum_{i=1}^{n} ME_{i,j}} \quad (9)$$

$$\text{FAR} = \frac{\sum_{i=1}^{n} FE_{i,j}}{\sum_{i=1}^{n} HE_{i,j} + \sum_{i=1}^{n} FE_{i,j}} \quad (10)$$

The critical success index (CSI) or threat score includes three possible situations and can range from 0 to 1, with 0 indicating complete failure and 1 indicating perfect performance. The probability of detection (POD) gives the likelihood that a pluvial flood will be observed with a correct warning, with 1 indicating that each of the pluvial floods has been correctly warned and 0 indicating that none of the pluvial floods have been detected by using rainfall thresholds. The false alarm ratio (FAR) is the ratio of false alarms to all events that trigger a warning. The FAR ranges from 0, indicating that no false alarms were generated, to 1, indicating that no flood events occurred and all of the warnings issued were false alarms.

3.3.2. Initial Boundary

The initial boundary affects how much computational time the model consumes. With a wide boundary range, the model can be computationally inefficient. However, with a narrow boundary, some optimal solutions might be ignored. Therefore, it is necessary to select an effective boundary in order to compute the optimal solutions effectively. The minimum boundary for duration at each station could be denoted as:

$$MinB_{i,D} = \left\{ \left(\min_{J=hazardous\ event} \{MCR_{i,J,D}\} \right) - 10 \right\},\ for\ D = 1,\ 3,\ 6,\ 12,\ 24, \quad (11)$$

where $MinB_{i,D}$ indicates the minimum boundary of the ith rain gauge with D-h duration. The maximum boundaries are determined by frequency analysis with a 5-year return period of rainfalls because the design capacity of the drainage systems for each district is based upon this return period. The frequency analysis can compute the annual maximum rainfall [57,58]. Five types of probability density function (PDF), namely, Gaussian Distribution (G), Lognormal Distribution (LN), Extreme Value Type 1 (EV1), Pearson Type III Distribution (PT3) and Log-Pearson Type III Distribution (LPT3), were selected for the frequency analysis in this study and the rainfall pattern of each rain gauge was arranged with a suitable PDF. Thus, the maximum boundaries for each station could be denoted as:

$$MaxB_{i,D,T} = u + \sigma K_T,\ for\ D = 1,\ 3,\ 6,\ 12,\ 24, \quad (12)$$

where T is the 5-year return period; u is the average value of D-h annual maximum cumulative rainfall; σ is the standard deviation of annual rainfall; and K_T is a frequency factor. The resulting maximum and minimum boundaries are shown in Figure 8.

3.3.3. Tabu Search (TS) for Rainfall Thresholds

TS, which was first proposed by Glover (1986), has the ability to escape the local solutions to reach the global optimal solution. Zheng et al. (1996) [59] applied TS to find the optimal flow and transport parameters in a groundwater model. Three years later, Zheng et al. (1999) [60] proposed an innovating method of TS that can be used to combine global optimal solutions in hydraulic problems. Tung and Chou (2002) [61] applied TS to optimize the parameters of groundwater simulation; their result shows that TS can find the best parameters for an optimal simulation. Li et al. (2006) [33] used TS to determine individual weights for rain gauges and estimate the seasonal rainfall. Leahy et al. (2008) [62] combined simulated annealing with TS to further optimize the parameters of artificial neural networks in predicting the river level. Huang et al. (2015) [32] applied TS in combination with a backpropagation neural network (BPNN) to compute the optimal planning solution for urban flood mitigation.

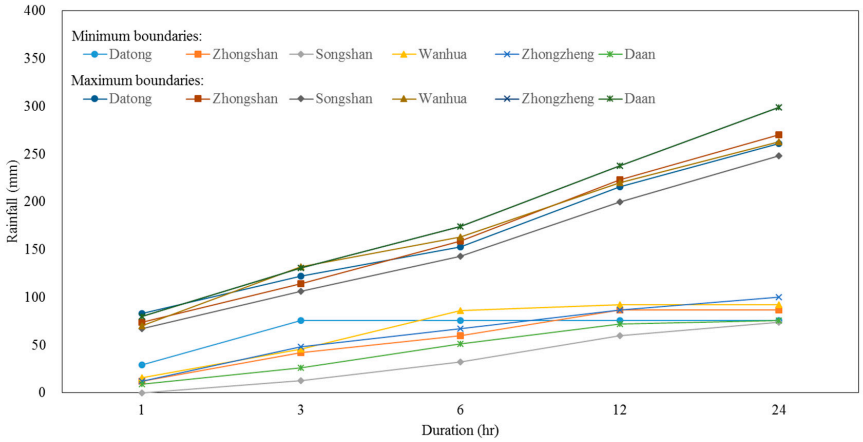

Figure 8. The minimum boundaries and maximum boundaries for rainfall thresholds.

Five parameters are adjusted for TS: the number of initial solutions, the number of iterations, the search space, the tabu list length and the stopping criterion. The number of initial solutions is 500 groups of rainfall thresholds. An infinite number of iterations is required in order to ensure that the neighborhood solutions of the criteria are no longer improving. The search space is one because the units of rainfall threshold are millimeters. The tabu list length is 25 rounds. The essence of a tabu list is to forbid repeating solutions; according to the rules, if a few groups of rainfall thresholds have the same criteria results, they will be forbidden with 25 rounds. The stopping criterion is such that if the neighborhood solutions are no longer improving, the algorithm will stop.

The objective function is given in Equation (8) through Equation (10). Equation (8) is considered firstly to optimize the rainfall thresholds because it can allow TS to widely search based on three situations with *Hit*, *Missed alarm* and *False alarm.* Then, with secondary priority given to Equation (9), TS can focus on the *Missed alarm* situation because a *Missed alarm* results in unwarned flooding. Lastly, Equation (10) is given tertiary priority because a *False alarm* is not as serious as a *Missed alarm* and Equation (10) simply enhances the confidence of rainfall threshold. Five variables (X_1, X_2, X_3, X_4 and X_5) represent the rainfall thresholds for different rain durations (1, 3, 6, 12 and 24 h). The constraints are shown in Equation (13) through Equation (22):

$$MinB_{i,1} < X_1 < MaxB_{i,1,5} \tag{13}$$

$$MinB_{i,3} < X_2 < MaxB_{i,3,5} \tag{14}$$

$$MinB_{i,6} < X_3 < MaxB_{i,6,5} \tag{15}$$

$$MinB_{i,12} < X_4 < MaxB_{i,12,5} \tag{16}$$

$$MinB_{i,24} < X_5 < MaxB_{i,24,5} \tag{17}$$

$$3X_1 > X_2 \tag{18}$$

$$2X_2 > X_3 \tag{19}$$

$$2X_3 > X_4 \tag{20}$$

$$2X_4 > X_5 \tag{21}$$

$$X_5 > X_4 > X_3 > X_2 > X_1 \tag{22}$$

The above equations illustrate the fact that the short- and long-duration rainfall thresholds are complementary to each other. The flowchart for the overall process is shown in Figure 9.

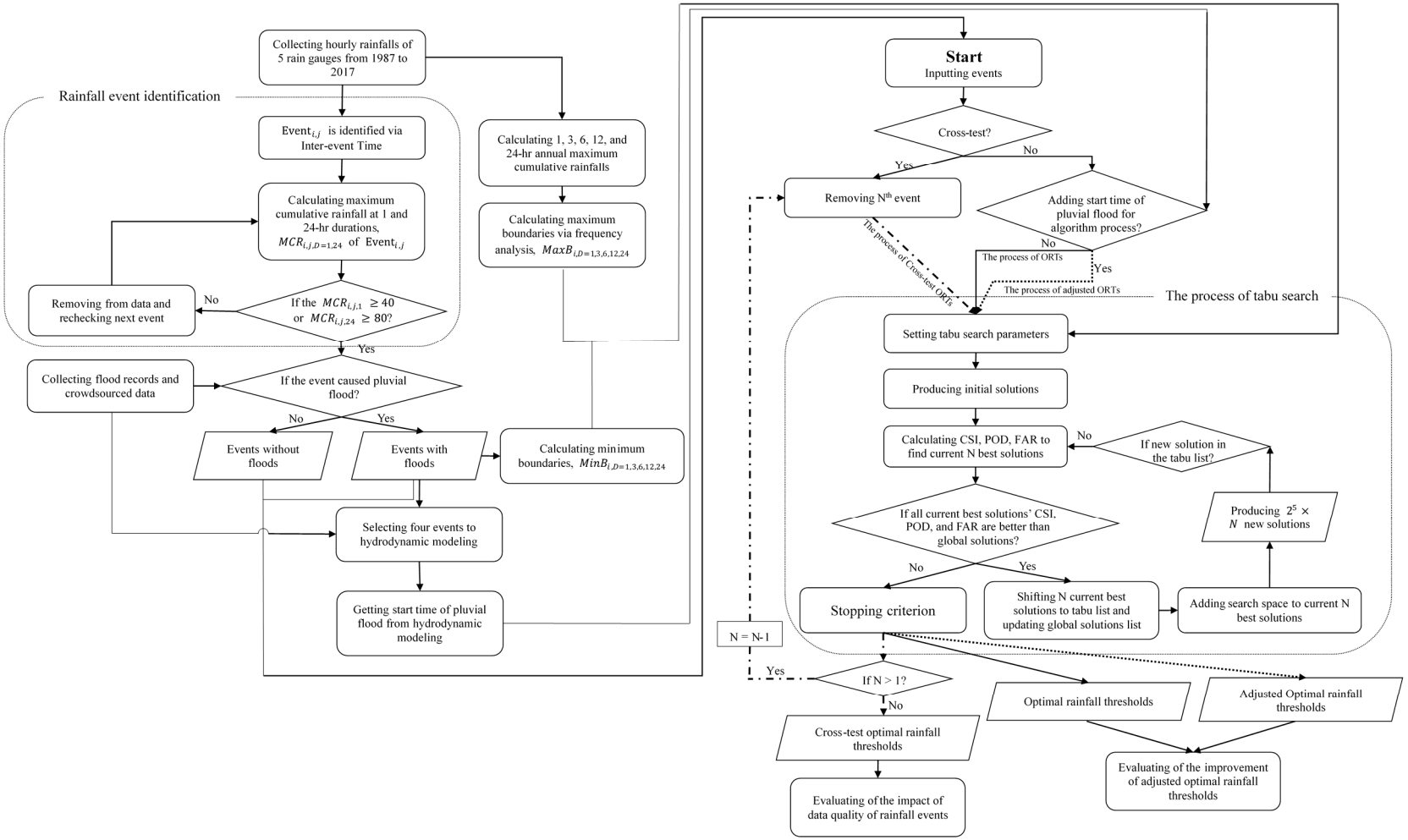

Figure 9. The flowchart of the study process.

4. Results and Discussion

4.1. Performance of TS and the Rainfall Threshold Model

The performance of TS for escaping local solutions to reach the optimal solution is illustrated in Figure 10. Figure 10a shows the results of CSI under constant values of ORTs with 6-, 12- and 24-h duration with variables of 1-h and 3-h rainfall thresholds at the Gongguan (C1A730) rain gauge in the Daan district. According to Figure 10a, TS is able to escape the local solutions located in the flat surface between 59 and 69 mm of the 1-h rainfall threshold and 95 and 121 mm of the 3-h rainfall threshold. Thus, TS was adopted to build the rainfall threshold model.

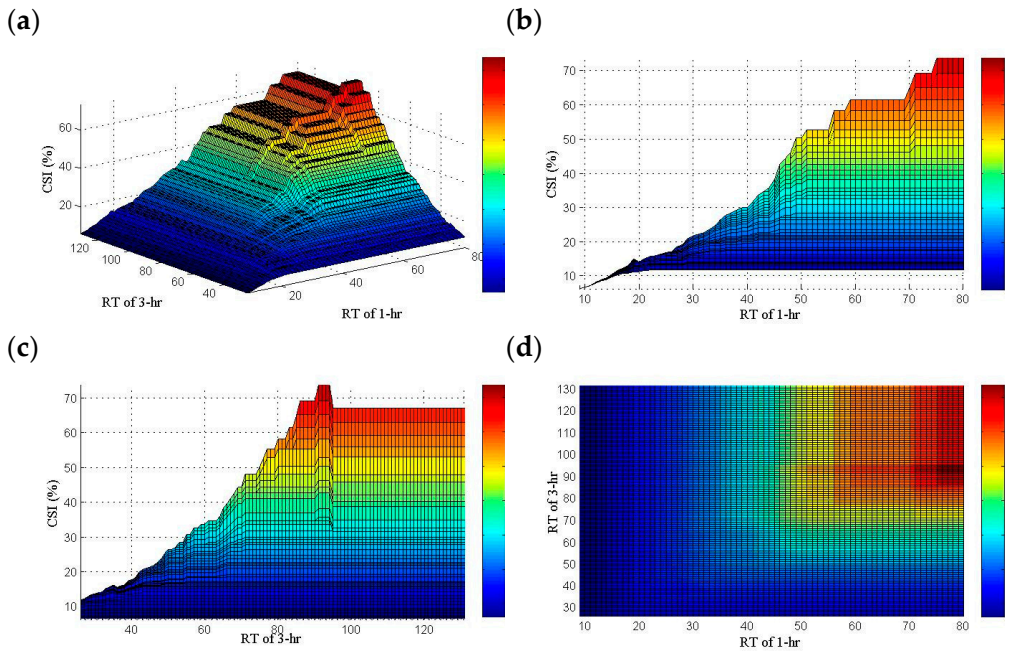

Figure 10. The CSI results at the Gongguan (C1A730) rain gauge in the Daan district: (**a**) the rainfall thresholds with 1-h and 3-h durations with constant values of ORTs with 6-, 12- and 24-h durations; (**b**) the rainfall threshold with 1-h duration; (**c**) the rainfall threshold with 3-h duration; (**d**) the rainfall threshold with 1-h and 3-h durations.

TS was used to optimize the rainfall thresholds at five rain gauges for warning six of the high inundation potential areas in central Taipei and the results, including ORTs, warning results of event number and performance of assessment criteria, are shown in Tables 4–6. The results show that the 1-h short-duration ORTs of the five rain gauges are higher than the WRTs, whereas the 3-h and 6-h ORTs are lower than the WRTs, except for the 3-h optimal rainfall threshold at the Jianguo rain gauge (Table 4). The differences between the ORTs and the WRTs of the 1-h, 3-h and 6-h durations are 1 to 15 mm, −23 to 8 mm and −46 to −3 mm, respectively. According to the warning ability of rainfall thresholds, the frequency of *False alarm* events and *Hit* events would decrease if the rainfall thresholds were to increase. Therefore, the ORTs could effectively represent the characteristics of the hazardous extreme rainfalls in central Taipei. As a result, rising 1-h rainfall threshold by TS could decrease *False alarms* more than *Hit* events because most of the non-flooding events are shorter than 3 h in central Taipei. In relation to the rise of 1-h ORT, the decrease of the 3-h and 6-h ORTs shows that the impacts of rainfall events longer than 3 h on floods are more significant to the city. For example, Typhoon Soudelor in 2015 would be alarmed by the 6-h ORT, as shown in Figure 11. Additionally, Typhoon Saola in 2012 would be alarmed by the 12-h ORT, whereas the WRA missed this flood event, as shown in Figure 12. These results indicate that the long-duration rainfall thresholds could improve the accuracy of flood warning.

Table 4. Optimal and adjusted rainfall thresholds of 1-, 3-, 6-, 12- and 24-h durations.

Warning District	Reference Rain Gauge	Optimal Rainfall Threshold of Each Duration					Difference between WRTs and ORTs					Adjusted Optimal Rainfall Threshold of Each Duration					Difference between WRTs and Adjusted ORTs				
		1 h	3 h	6 h	12 h	24 h	1 h	3 h	6 h	12 h	24 h	1 h	3 h	6 h	12 h	24 h	1 h	3 h	6 h	12 h	24 h
Datong	Taiping	61	98	142	214	259	1	−12	−18	-	-	61	98	142	191	245	1	−12	−18	-	-
Zhongshan	Jianguo	67	108	114	119	232	7	8	−36	-	-	65	69	110	116	211	5	−31	−40	-	-
Songshan	Minsheng	65	97	124	164	221	5	−13	−46	-	-	57	75	109	140	233	−3	−35	−61	-	-
Wanhua	Shuangyuan	61	97	147	173	191	1	−23	−3	-	-	61	85	87	192	218	1	−35	−63	-	-
Zhongzheng	Gongguan	76	103	135	152	257	16	−17	−15	-	-	75	98	135	207	252	15	−22	−15	-	-
Daan	Gongguan	75	91	106	149	192	15	−9	−34	-	-	75	91	106	133	284	15	−9	−34	-	-

Table 5. Warning results of optimal rainfall thresholds (ORTs), adjusted ORTs and WRTs.

Warning District	Reference Rain Gauge	WRTs for Flood Warning				ORTs for Flood Warning				Adjusted ORTs for Flood Warning			
		A	B	C	D	A	B	C	D	A	B	C	D
Datong	Taiping	5	1	2	679	5	1	1	680	5	1	1	680
Zhongshan	Jianguo	4	6	3	692	9	1	5	690	10	0	6	689
Songshan	Minsheng	5	5	1	720	7	3	2	719	8	2	4	717
Wanhua	Shuangyuan	5	3	3	703	7	1	1	705	8	0	5	701
Zhongzheng	Gongguan	6	3	4	945	7	2	3	946	6	3	1	948
Daan	Gongguan	6	6	4	942	11	1	3	943	11	1	2	944

A: Hit; B: Missed alarm; C: False alarm; D: Correct rejection.

Table 6. Performance of the ORTs, adjusted ORTs and WRTs evaluated in terms of probability of detection (POD), false alarm ratio (FAR) and critical success index (CSI).

Warning District	Reference Rain Gauge	WRTs For Flood Warning			ORTs for Flood Warning			Adjusted ORTs for Flood Warning		
		CSI	POD	FAR	CSI	POD	FAR	CSI	POD	FAR
Datong	Taiping	0.625	0.833	0.286	0.714	0.833	0.167	0.714	0.833	0.167
Zhongshan	Jianguo	0.308	0.400	0.429	0.600	0.900	0.357	0.625	1.000	0.375
Songshan	Minsheng	0.455	0.500	0.167	0.583	0.700	0.222	0.571	0.800	0.333
Wanhua	Shuangyuan	0.455	0.625	0.375	0.778	0.875	0.125	0.615	1.000	0.385
Zhongzheng	Gongguan	0.462	0.667	0.400	0.583	0.778	0.300	0.600	0.667	0.143
Daan	Gongguan	0.375	0.500	0.400	0.733	0.917	0.214	0.786	0.917	0.154

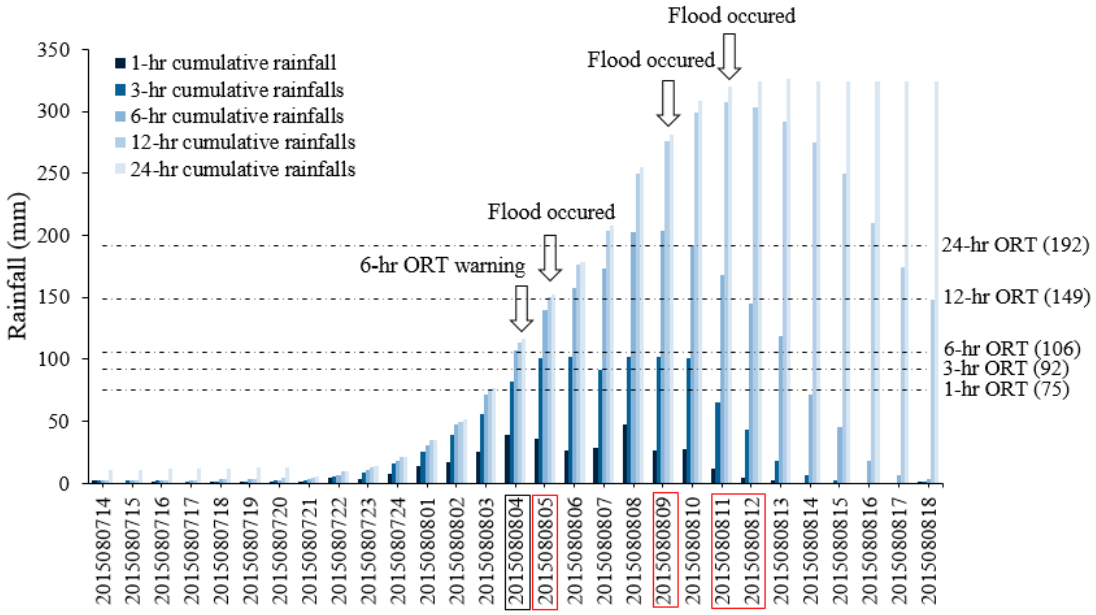

Figure 11. The warning process for the Gongguan (C1A730) rain gauge during Typhoon Soudelor in the Daan district.

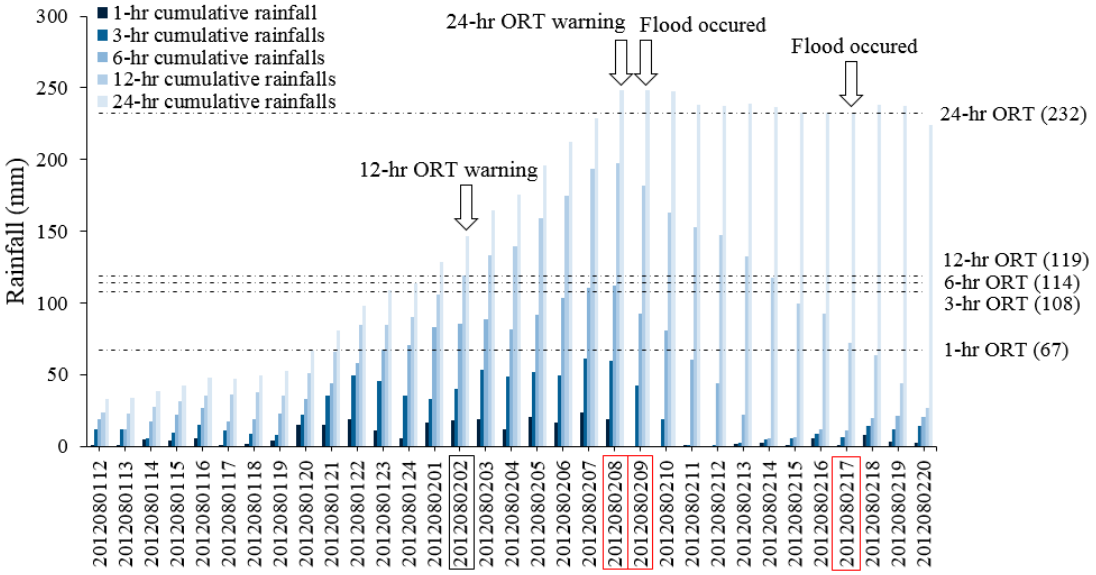

Figure 12. The warning process for the Jianguo (A1AB50) rain gauge during Typhoon Saola in the Zhongshan district.

In Table 5, the warning results show that the ORTs make it possible to increase the number of flood warning events and reduce the number of *False alarm* events. For the Taiping rain gauge in the Datong district, the performances of the ORTs and the WRTs are almost the same. For the other districts, the frequency of *Hit* events could be improved by ORTs. The greatest improvements in the number of *Hit* events occurred at the Gongguan rain gauge in the Daan district and at the Jianguo rain gauge in the Zhongshan district. The numbers of *Hit* events improved from 6 to 11 for the Daan district and from 4 to 9 for the Zhongshan district. The CSI, POD and FAR criteria are presented in Table 6 to quantify the performances of different rainfall thresholds. Because POD is the ratio of *Hit* events to all flood events, the increase of *Hit* events would enhance the POD more significantly based on fewer flood events as evidenced by the changes in the Daan and Zhongshan districts. Both of those districts have five more *Hit* events via ORT but the POD of the Daan district is higher than that of

the Zhongshan district. Also, the overall performances in terms of CSI, POD and FAR of the ORTs are better than those of the WRTs. In the Daan district, the ORTs improve CSI by 95.6% (from the 0.375 of the WRTs to the 0.733 of the ORTs). Meanwhile, POD and FAR are improved by 125.0% in the Zhongshan district and 66.7% in the Wanhua district, respectively.

4.2. The Impacts of Data Quality on the Rainfall Threshold Model via TS

The study evaluates the impact of data quality on rainfall thresholds by a cross test that retests the rainfall thresholds by TS using a part of flood events except for a single event in rotation. The cross test results in terms of ORTs, POD, FAR, CSI, warning results and the warning process are shown in Tables 7–10. The results show that the characteristics of rainfalls are the dominant factor in the performance of the TS optimization.

Table 7. Warning process results of the cross test for the six districts with partial flood events.

No.	Event	Date	Datong	Zhongshan			Songshan			Wanhua		Zhongzheng			Daan		
			E10	E03	T04	T09	T02	E08	T06	T03	T04	E10	E03	T04	T09	T02	E08
E01	Heavy rain 0502	2012/05/02															
E02	Heavy rain 0610	2012/06/10		1	1	1	0	0	0	1	0				1	0	1
T01	Typhoon Saola	2012/08/02		1	1	1						−1	0	0	−1	0	0
T02	Typhoon Soulik	2013/07/11					−1	0	0						0	−1	0
E03	Heavy rain 0814	2013/08/14	0	−1	1	0				1	0						
T03	Typhoon Trami	2013/08/20		1	1	1	0	1	0	−1	0				1	0	1
E04	Heavy rain 0822	2013/08/22	0							0	0	0	0	0	1	0	0
T04	Typhoon Kong-rey	2013/08/28		0	−1	0				1	−1	0	−1	0			
T05	Typhoon Fitow	2013/10/06															
E05	Heavy rain 0515	2014/05/15															
E06	Heavy rain 0519	2014/05/19		1	1	1	0	1	0	0	0	1	0	0	1	0	1
E07	Heavy rain 0605	2014/06/05					0	0	0								
E08	Heavy rain 0614	2015/06/14					0	−1	0			1	0	1	0	0	0
T06	Typhoon Chan-hom	2015/07/09					0	1	−1								
E09	Heavy rain 0723	2015/07/23	0	1	1	−1											
T07	Typhoon Soudelor	2015/08/07	0	1	1	1				0	0	1	0	0	1	0	0
E10	Heavy rain 0818	2015/08/18	−1												1	0	−1
E11	Heavy rain 0827	2015/08/27										0	0	−1			
T08	Typhoon Dujuan	2015/09/28					0	0	0			0	0	0			
E12	Heavy rain 0617	2016/06/17					0	1	0						1	0	0
T09	Typhoon Megi	2016/09/25		0	0	1									1	0	0
E13	Heavy rain 0602	2017/06/02	0	1	1	1	1	1	0	1	0	0	0	0	1	0	0
E14	Heavy rain 0613	2017/06/13															

1: Hit; 0: Missed alarm; −1: Removed Event.

At the Taiping (A1A9X0) rain gauge in the Datong district, each optimal rainfall threshold is unable to alert for Heavy rain 0818 in 2015 (Table 7) because the cumulative rainfalls of the event are insufficient. A similar situation occurs with the floods induced by Typhoon Soulik in 2013 in the Daan district, Typhoon Kong-rey in 2013 in the Wanhua and Zhongzheng districts and Typhoon Chan-hom in 2015 in the Songshan district.

Some flood events have high cumulative rainfalls. If these events were not considered during the optimization, the TS would produce low rainfall thresholds. For example, the maximum cumulative rainfall values of Heavy rain 0602 in 2017 are 80 mm/h and 140 mm/3 h, the largest among the events, so the values of ORTs produced by the optimization without Heavy rain 0602 for 1-, 3-, 6- and 24-h durations are the smallest among those in the Songshan district. Therefore, although Typhoon Soulik in 2012 only brought 79-mm rainfalls in 6 h in the Songshan district, it still could be alerted via the 6-h rainfall threshold (72 mm), as shown in Table 7. In addition, Heavy rain 0614 in 2015 had the highest cumulative rainfall of all the events (105 mm/h; 188 mm/3 h); the values of the 3-h optimal rainfall threshold (86 mm) produced by the optimization without that event are the smallest among the other rainfall thresholds in the Zhongzheng district. These results show that the values of ORTs would become small because small cumulative rainfalls from flood events limit the ability of TS to find appropriate ORTs.

Table 8. ORTs with cross test.

No.	Event	Date	Datong					Zhongshan					Songshan					Wanhua					Zhongzheng					Daan				
			1 h	3 h	6 h	12 h	24 h	1 h	3 h	6 h	12 h	24 h	1 h	3 h	6 h	12 h	24 h	1 h	3 h	6 h	12 h	24 h	1 h	3 h	6 h	12 h	24 h	1 h	3 h	6 h	12 h	24 h
E01	Heavy rain 0502	2012/05/02																														
E02	Heavy rain 0610	2012/06/10						48	76	93	103	204	66	96	124	156	181	61	91	157	175	185						75	91	101	176	282
T01	Typhoon Saola	2012/08/02						65	71	110	117	265											75	120	162	204	260	75	91	164	168	251
T02	Typhoon Soulik	2013/07/11											64	95	116	188	205											75	91	154	175	214
E03	Heavy rain 0814	2013/08/14	77	101	134	181	231	68	109	130	144	148						61	99	150	167	198										
T03	Typhoon Trami	2013/08/20						65	69	111	116	173	60	75	104	161	225	67	98	155	197	203						76	91	107	140	214
E04	Heavy rain 0822	2013/08/22	61	104	147	208	254											66	119	151	191	259	78	106	150	234	246	75	94	136	157	236
T04	Typhoon Kong-rey	2013/08/28						71	107	136	161	198						61	97	150	188	191	76	118	144	211	290					
T05	Typhoon Fitow	2013/10/06																														
E05	Heavy rain 0515	2014/05/15																														
E06	Heavy rain 0519	2014/05/19						67	84	110	117	177	64	75	133	193	246	66	119	154	168	256	79	126	127	200	203	80	91	106	134	255
E07	Heavy rain 0605	2014/06/05											65	98	135	181	243															
E08	Heavy rain 0614	2015/06/14											65	95	103	162	197						76	86	135	154	232	78	91	167	178	239
T06	Typhoon Chan-hom	2015/07/09											64	75	98	151	233															
E09	Heavy rain 0723	2015/07/23	68	120	152	184	251	65	73	110	116	199																				
T07	Typhoon Soudelor	2015/08/07	64	105	139	197	239	56	85	100	107	264						67	94	161	211	212	75	104	155	174	195	76	93	124	133	293
E10	Heavy rain 0818	2015/08/18	61	99	135	183	231																					75	91	131	136	255
E11	Heavy rain 0827	2015/08/27																					76	113	172	190	215					
T08	Typhoon Dujuan	2015/09/28											66	99	118	183	187						75	99	137	213	252					
E12	Heavy rain 0617	2016/06/17											61	75	109	144	179											75	99	135	152	257
T09	Typhoon Megi	2016/09/25						71	103	150	191	204																75	92	135	160	216
E13	Heavy rain 0602	2017/06/02	67	101	149	211	237	65	75	93	105	268	57	67	72	149	171	61	102	159	166	176	76	123	141	229	288	75	91	149	159	218
E14	Heavy rain 0613	2017/06/13																														

Table 9. Performance of cross test as evaluated by the criteria POD, FAR and CSI.

No.	Event	Date	Datong			Zhongshan			Songshan			Wanhua			Zhongzheng			Daan		
			CSI	POD	FAR	CSI	POD	FAR	CSI	POD	FAR	CSI	POD	FAR	CSI	POD	FAR	CSI	POD	FAR
E01	Heavy rain 0502	2012/05/02																		
E02	Heavy rain 0610	2012/06/10				0.529	1.000	0.471	0.545	0.667	0.250	0.750	0.857	0.143				0.714	0.909	0.231
T01	Typhoon Saola	2012/08/02				0.643	1.000	0.357							0.667	0.750	0.143	0.750	0.818	0.100
T02	Typhoon Soulik	2013/07/11							0.636	0.778	0.222							0.750	0.818	0.100
E03	Heavy rain 0814	2013/08/14	0.667	0.800	0.200	0.571	0.889	0.385				0.750	0.857	0.143						
T03	Typhoon Trami	2013/08/20				0.600	1.000	0.400	0.538	0.778	0.364	0.750	0.857	0.143				0.769	0.909	0.167
E04	Heavy rain 0822	2013/08/22	0.667	0.800	0.200							0.625	0.714	0.167	0.500	0.625	0.286	0.750	0.818	0.100
T04	Typhoon Kong-rey	2013/08/28				0.583	0.778	0.300				0.875	1.000	0.125	0.667	0.750	0.143			
T05	Typhoon Fitow	2013/10/06																		
E05	Heavy rain 0515	2014/05/15																		
E06	Heavy rain 0519	2014/05/19				0.600	1.000	0.400	0.636	0.778	0.222	0.625	0.714	0.167	0.500	0.750	0.400	0.769	0.909	0.167
E07	Heavy rain 0605	2014/06/05							0.600	0.667	0.143									
E08	Heavy rain 0614	2015/06/14							0.583	0.778	0.300				0.583	0.875	0.364	0.667	0.727	0.111
T06	Typhoon Chan-hom	2015/07/09							0.615	0.889	0.333									
E09	Heavy rain 0723	2015/07/23	0.667	0.800	0.200	0.600	1.000	0.400												
T07	Typhoon Soudelor	2015/08/07	0.667	0.800	0.200	0.563	1.000	0.438				0.625	0.714	0.167	0.500	0.750	0.400	0.692	0.818	0.182
E10	Heavy rain 0818	2015/08/18	0.833	1.000	0.167													0.769	0.909	0.167
E11	Heavy rain 0827	2015/08/27													0.600	0.750	0.250			
T08	Typhoon Dujuan	2015/09/28							0.545	0.667	0.250				0.556	0.625	0.167			
E12	Heavy rain 0617	2016/06/17							0.538	0.778	0.364							0.750	0.818	0.100
T09	Typhoon Megi	2016/09/25				0.636	0.778	0.222										0.750	0.818	0.100
E13	Heavy rain 0602	2017/06/02	0.667	0.800	0.200	0.600	1.000	0.400	0.533	0.889	0.429	0.750	0.857	0.143	0.556	0.625	0.167	0.750	0.818	0.100
E14	Heavy rain 0613	2017/06/13																		

Table 10. Warning results of the cross test for the six districts.

No.	Event	Date	Datong				Zhongshan				Songshan.				Wanhua				Zhongzheng				Daan			
			A	B	C	D	A	B	C	D	A	B	C	D	A	B	C	D	A	B	C	D	A	B	C	D
E01	Heavy rain 0502	2012/05/02																								
E02	Heavy rain 0610	2012/06/10					9	0	8	687	6	3	2	719	6	1	1	705					10	1	3	943
T01	Typhoon Saola	2012/08/02					9	0	5	690									6	2	1	948	9	2	1	945
T02	Typhoon Soulik	2013/07/11									7	2	2	719									9	2	1	945
E03	Heavy rain 0814	2013/08/14	4	1	1	680	8	1	5	690					6	1	1	705								
T03	Typhoon Trami	2013/08/20					9	0	6	689	7	2	4	717	6	1	1	705					10	1	2	944
E04	Heavy rain 0822	2013/08/22	4	1	1	680									5	2	1	705	5	3	2	947	9	2	1	945
T04	Typhoon Kong-rey	2013/08/28					7	2	3	692					7	0	1	705	6	2	1	948				
T05	Typhoon Fitow	2013/10/06																								
E05	Heavy rain 0515	2014/05/15																								
E06	Heavy rain 0519	2014/05/19					9	0	6	689	7	2	2	719	5	2	1	705	6	2	4	945	10	1	2	944
E07	Heavy rain 0605	2014/06/05									6	3	1	72												
E08	Heavy rain 0614	2015/06/14									7	2	3	718					7	1	4	945	8	3	1	945
T06	Typhoon Chan-hom	2015/07/09									8	1	4	717												
E09	Heavy rain 0723	2015/07/23	4	1	1	680	9	0	6	689																
T07	Typhoon Soudelor	2015/08/07	4	1	1	680	9	0	7	688					5	2	1	705	6	2	4	945	9	2	2	944
E10	Heavy rain 0818	2015/08/18	5	0	1	680																	10	1	2	944
E11	Heavy rain 0827	2015/08/27																	6	2	2	947				
T08	Typhoon Dujuan	2015/09/28									6	3	2	719					5	3	1	948				
E12	Heavy rain 0617	2016/06/17									7	2	4	717									9	2	1	945
T09	Typhoon Megi	2016/09/25					7	2	2	693													9	2	1	945
E13	Heavy rain 0602	2017/06/02	4	1	1	680	9	0	6	689	8	1	6	715	6	1	1	705	5	3	1	948	9	2	1	945
E14	Heavy rain 0613	2017/06/13																								

A: Hit; B: Missed alarm; C: False alarm; D: Correct rejection.

In contrast, without flood events that have low cumulative rainfalls, TS will find higher values of ORTs. In Table 7, the ORTs in the Zhongshan district show that the values of ORTs produced by an optimization without Heavy rain 0814 in 2013, Typhoon Kong-rey in 2013 or Typhoon Megi in 2016 are larger than the others due to the relatively small cumulative rainfalls. The minimum cumulative rainfalls of 1-, 3-, 6- and 12-h durations are 22 mm, 52 mm (Typhoon Megi), 70 mm (Typhoon Kong-rey) and 97 mm (Heavy rain 0814), respectively. Therefore, the maximum rainfall thresholds would appear in each optimization as shown in Table 8. These results show that the rainfall thresholds produced by optimizations without the smaller cumulative rainfalls would be rather large because the small rainfalls influence the TS. Without the constrictive effect of the small rainfalls, TS is allowed to produce high values of rainfall thresholds.

Furthermore, although Heavy rain 0822 in 2013, Heavy rain 0519 in 2014 and Typhoon Soudelor in 2015 do not have particularly large or low cumulative rainfalls among all events, these three events are more sensitive than others for alerting Typhoon Trami in 2013 in the Wanhua district. In fact, the rain gauge at Shuangyuan (A1AB20) is unable to alert the typhoon if the optimization is performed without those three flood events, as shown in Table 7. Furthermore, as shown in Tables 9 and 10, the *Hit*, CSI, POD and FAR values of the three events are the same or worse at 5, 0.625, 0.714 and 0.167, respectively. Consequently, those events are also important for the ability of TS to find ORTs.

4.3. Improvement Gained by Applying Hydrodynamic Modeling to the Rainfall Threshold Model

The SOBEK model is applied to simulate hydrodynamics for the relationship between rainfall and urban floods and to find the start time of manhole overflowing. The concept of applying the start time of manhole flooding to the rainfall threshold model is illustrated in Figure 13. In Figure 13, each observed rainfall before the start time of manhole flooding is important to the ability to issue a warning in time. Therefore, the start time of manhole flooding could help to identify the crucial rainfall period for optimizing the rainfall thresholds.

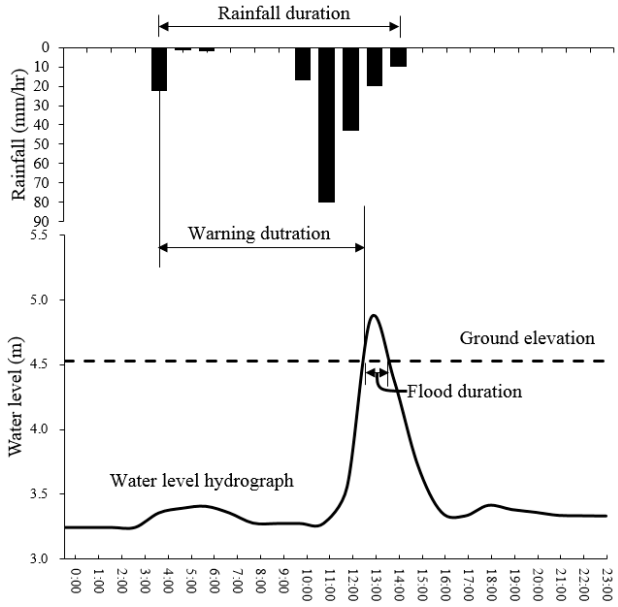

Figure 13. The relationship between warning, rainfall and flood duration.

In this study, the flooding processes of four flood events are simulated by the hydrodynamic modeling due to the relatively large flooding areas. The four simulated events with start time of manhole flooding and other flood events are all considered in the TS to find the adjusted ORTs. The start times of manhole flooding are shown in Table 11. Heavy rain 0723 is a thundershower with a short duration and the flood occurred quickly, within 3 h in the Datong, Zhongshan and Daan districts.

Induced by a Mei-yu front, Heavy rain 0519 and Heavy rain 0602 have long rainfall durations and flooding occurred within 8 to 19 h. The earliest start time of manhole flooding of Typhoon Soudelor for each district is approximately 8 to 19 h after the rain event begins.

Table 11. The hydrodynamic modeling output for each event's start time of manhole flooding after the onset of rainfall for the six districts.

No.	Event	Warning District					
		Datong	Zhongshan	Songshan	Wanhua	Zhongzheng	Daan
E06	Heavy rain 0519	18	18	17	20	21	
E09	Heavy rain 0723	3	3				1
T07	Typhoon Soudelor	16	9	8	8	15	19
E13	Heavy rain 0602	9	9	10	11	11	11

Units: hours.

Table 12 shows the difference in alert time between the ORTs and the adjusted ORTs. The results reveal that adding the start time of manhole flooding from the flood routing simulation to TS could improve the early warning time. The improvement of warning time is from 1 to 3 h ahead and some flood events can be altered after adjusting the ORTs. Except for the Zhongzheng district in which one event is missed and has a shorter warning time, most of the districts have better performance in warning time with the adjusted ORTs than with the original ORTs. The maximum improvement of warning time is 3 h, which occurred for Heavy rain 0610 in 2012 in the Zhongshan, Songshan and Wanhua districts, Heavy rain 0519 in 2014 in the Zhongshan district and Typhoon Soudelor in 2015 in the Wanhua district. There was a 2-h improvement in warning time for Heavy rain 0519 in 2014 and Heavy rain 0605 in 2014 in the Songshan district. The majority of events had a 1-h improvement in warning time. Three additional flood events could be altered by adjusting the ORTs; those events are Heavy rain 0814 in 2013 in the Zhongshan district, Typhoon Kong-rey in 2013 in the Wanhua district and Heavy rain 0614 in 2015 in the Songshan district.

Table 12. The improvements in early warning time in the adjusted vs. original ORTs.

No.	Event	Date	Datong	Zhongshan	Songshan	Wanhua	Zhongzheng	Daan
E01	Heavy rain 0502	2012/05/02						
E02	Heavy rain 0610	2012/06/10		3	3	3		0
T01	Typhoon Saola	2012/08/02		0			No alert	1
T02	Typhoon Soulik	2013/07/11			X			X
E03	Heavy rain 0814	2013/08/14	0	Alert		0		
T03	Typhoon Trami	2013/08/20		0	1	1		0
E04	Heavy rain 0822	2013/08/22	0			0	0	0
T04	Typhoon Kong-rey	2013/08/28		1		Alert	X	
T05	Typhoon Fitow	2013/10/06						
E05	Heavy rain 0515	2014/05/15						
E06	Heavy rain 0519	2014/05/19		3	2	0	−1	0
E07	Heavy rain 0605	2014/06/05			2			
E08	Heavy rain 0614	2015/06/14			Alert		0	0
T06	Typhoon Chan-hom	2015/07/09			X			
E09	Heavy rain 0723	2015/07/23	0	0				
T07	Typhoon Soudelor	2015/08/07	0	1		3	0	0
E10	Heavy rain 0818	2015/08/18	X					0
E11	Heavy rain 0827	2015/08/27					X	
T08	Typhoon Dujuan	2015/09/28			1		0	
E12	Heavy rain 0617	2016/06/17			1			0
T09	Typhoon Megi	2016/09/25		0				0
E13	Heavy rain 0602	2017/06/02	0	0	0	0	0	0
E14	Heavy rain 0613	2017/06/13						

Alert: Adjusted produces alert but original does not; No alert: Adjusted does not produce alert but original does; X: Neither produce alert.

5. Conclusions

Herein, a method for pluvial flood warning via rainfall thresholds has been developed for central Taipei, using the TS algorithm to optimize the rainfall thresholds. The results of the study show that

ORTs have better performance on warning issues than WRTs and the adjusted ORTs produce even more warning time. However, the ORTs are influenced by some particular events, as evidenced by the cross test. These influences will need to be carefully accounted for. As measured by the assessment criteria CSI and POD, the overall adjusted ORTs have better performances than the ORTs and WRTs. Furthermore, with the small 3- and 6-h ORTs, the chances of advanced warning for pluvial floods are substantially improved. Also, the adjusted ORTs based on hydrodynamic modeling simulating the start time of manhole flooding produce more warning time than ORTs. The maximum improvement in warning time is 3 h and some flood events can be altered after adjusting the ORTs. Therefore, by applying TS and a hydrodynamic modeling adjustment, the flood warning system for central Taipei could be substantially improved. In future studies, radar data could be applied to improve the observations of the rain gauge network for the rainfall threshold model; this might be beneficial because we found that the spatial distribution of some extreme rainfall events is uneven and the rain gauge network could not always detect the "hot zone" of a hazardous area.

Author Contributions: H.-Y.L. developed the rainfall thresholds model and took the lead in writing the manuscript. T.-Y.P. designed the study, revised the manuscript and supervised the research work. H.-K.C. performed the hydrodynamic modeling and provided results. C.-T.H. provide crowdsourced data and analyzed the data. J.-S.L. revised the manuscript and supervised the research work. Y.-C.T. and M.-D.S. offered guidance and suggestion to the manuscript.

Funding: This study is funded by Ministry of Science and Technology, Taiwan, under Grants MOST 107-2625-M-009-005 and MOST 107-2628-M-002-016.

Acknowledgments: The authors would like to gratefully acknowledge the support data from the Central Weather Bureau and the Water Resources Agency in Taiwan. In addition, the authors appreciate the Hydrotech Research Institute of National Taiwan University, the Center for Weather Climate and Disaster Research of National Taiwan University and Research Center for Climate Change and Sustainable Development of National Taiwan University for their facilities and support.

Conflicts of Interest: The authors declare no conflict of interest.

References

1. Wu, D.; Wang, Y. A research on using critical precipitation value for Taiwan inundation warning system. In Proceedings of the 2009 Conference for Disaster Management in Taiwan, Taipei, Taiwan, 19 December 2009.
2. Hsu, T.W.; Shih, D.S.; Chen, W.J. Destructive flooding induced by broken embankments along Linbian Creek, Taiwan, during Typhoon Morakot. *J. Hydrol. Eng.* **2015**, *20*, 05014025. [CrossRef]
3. Niedźwiedź, T.; Łupikasza, E.; Pińskwar, I.; Kundzewicz, Z.W.; Stoffel, M.; Małarzewski, Ł. Variability of high rainfalls and related synoptic situations causing heavy floods at the northern foothills of the Tatra Mountains. *Appl. Clim.* **2015**, *119*, 273–284. [CrossRef]
4. Jhong, Y.D.; Chen, C.S.; Lin, H.P.; Chen, S.T. Physical hybrid neural network model to forecast typhoon floods. *Water* **2018**, *10*, 632. [CrossRef]
5. Stephenson, V.; Finlayson, A.; Morel, L.M. A risk-based approach to shelter resilience following flood and typhoon damage in rural Philippines. *Geosciences* **2018**, *8*, 76. [CrossRef]
6. Saeed, G.; Bahram, S.; Reza, M. Derivation of probabilistic thresholds of spatially distributed rainfall for flood forecasting. *Water Resour. Manag.* **2010**, *24*, 3547–3559.
7. Jang, J.H. An advanced method to apply multiple rainfall thresholds for urban flood warnings. *Water* **2015**, *7*, 6056–6078. [CrossRef]
8. Mirus, B.B.; Becker, R.E.; Baum, R.L.; Smith, J.B. Integrating real-time subsurface hydrologic monitoring with empirical rainfall thresholds to improve landslide early warning. *Landslides* **2018**, *15*, 1909–1919. [CrossRef]
9. Pan, H.L.; Jiang, Y.J.; Wang, J.; Ou, G.Q. Rainfall threshold calculation for debris flow early warning in areas with scarcity of data. *Nat. Hazards Earth Syst. Sci.* **2018**, *18*, 1395–1409. [CrossRef]
10. Saito, H.; Murakami, W.; Daimaru, H.; Oguchi, T. Effect of forest clear-cutting on landslide occurrences: Analysis of rainfall thresholds at Mt. Ichifusa, Japan. *Geomorphology* **2017**, *276*, 1–7. [CrossRef]

11. Candela, A.; Aronica, G.T. Rainfall thresholds derivation for warning pluvial flooding risk in urbanised areas. In Proceedings of the 3rd European Conference on Flood Risk Management, Lyon, France, 17–21 October 2016.
12. Douinot, A.; Roux, H.; Garambois, P.A.; Larnier, K.; Labat, D.; Dartus, D. Accounting for rainfall systematic spatial variability in flash flood forecasting. *J. Hydrol.* **2016**, *541*, 359–370. [CrossRef]
13. Yin, J.; Yu, D.; Yin, Z.; Liu, M.; He, Q. Evaluating the impact and risk of pluvial flash flood on intra-urban road network: A case study in the city center of Shanghai, China. *J. Hydrol.* **2016**, *537*, 138–145. [CrossRef]
14. Yang, T.H.; Hwang, G.D.; Tsai, C.C.; Ho, J.Y. Using rainfall thresholds and ensemble precipitation forecasts to issue and improve urban inundation alerts. *Hydrol. Earth Syst. Sci.* **2016**, *20*, 4731–4745. [CrossRef]
15. Georgakakos, K.P. Analytical results for operational flash flood guidance. *J. Hydrol.* **2006**, *317*, 81–103. [CrossRef]
16. Alfieri, L.; Salamaon, P.; Pappernberger, F.; Wetterhall, F.; Thielen, J. Operational early warning systems for water-related hazards in Europe. *Environ. Sci. Policy* **2012**, *21*, 35–49. [CrossRef]
17. Martina, M.L.V.; Todini, E.; Libralon, A. A Bayesian decision approach to rainfall thresholds based flood warning. *Hydrol. Earth Syst. Sci.* **2006**, *10*, 413–426. [CrossRef]
18. Wu, S.; Hsu, C.; Lien, H.; Chang, C. Modeling the effect of uncertainties in rainfall characteristics on flash flood warning based on rainfall thresholds. *Nat. Hazards* **2015**, *75*, 1677–1711. [CrossRef]
19. Sinclair, M. Comparison of the performance of modern heuristics for combinatorial optimization on real data. *Comput. Oper. Res.* **1993**, *20*, 687–695. [CrossRef]
20. Malek, M.; Guruswamy, M.; Pandya, M. Serial and parallel simulated annealing and tabu search algorithms for the traveling salesman problem. *Ann. Oper. Res.* **1989**, *21*, 59–84. [CrossRef]
21. Arostegui, M.A., Jr.; Kadipasaoglu, S.N.; Khumawala, B.M. An empirical comparison of Tabu Search, Simulated Annealing and Genetic Algorithms for facilities location problems. *Int. J. Prod. Econ.* **2006**, *103*, 742–754. [CrossRef]
22. Lidbe, A.D.; Hainen, A.M.; Jones, S.L. Comparative study of simulated annealing, tabu search and the genetic algorithm for calibration of the microsimulation model. *Trans. Soc. Model. Simul. Int.* **2017**, *93*, 21–33. [CrossRef]
23. Glover, F. Future paths for integer programming and links to artificial intelligence. *Comput. Oper. Res.* **1986**, *13*, 533–549. [CrossRef]
24. Glover, F. Tabu search—Part 1. *Orsa J. Comput.* **1989**, *1*, 190–206. [CrossRef]
25. Glover, F. Tabu search—Part 2. *Orsa J. Comput.* **1990**, *2*, 4–32. [CrossRef]
26. Glover, F.; Laguna, M. *Tabu Search*; Kluwer Academic: Boston, TX, USA, 1997.
27. Tan, C.C.; Tung, C.P.; Tsai, F.T.C. Applying zonation methods and tabu search to improve the ground-water modeling. *J. Am. Water Resour. Assoc.* **2008**, *44*, 108–120. [CrossRef]
28. Moutsopoulos, K.N.; Papaspyros, J.N.E.; Tsihrintzis, V.A. Management of groundwater resources using surface pumps: Optimization using genetic algorithms and the tabu search method. *KSCE J. Civ. Eng.* **2017**, *21*, 2968–2976. [CrossRef]
29. Yang, Y.; Wu, J.; Wang, J.; Zhou, Z. An elitist multiobjective tabu search for optimal design of groundwater remediation systems. *Groundwater* **2017**, *55*, 811–826. [CrossRef]
30. Kangrang, A.; Prasanchum, H.; Hormwichian, R. Development of future rule curves for multipurpose reservoir operation using conditional genetic and tabu search algorithms. *Adv. Civ. Eng.* **2018**. [CrossRef]
31. Alsmadi, M.K. Forecasting river flow in the USA using a hybrid metaheuristic algorithm with back-propagation algorithm. *Sci. J. King Faisal Univ. (Basic Appl. Sci.)* **2017**, *18*, 13–24.
32. Huang, C.L.; Hsu, N.S.; Wei, C.C.; Luo, W.J. Optimal spatial design of capacity and quantity of rainwater harvesting systems for urban flood mitigation. *Water* **2015**, *7*, 5173–5202. [CrossRef]
33. Li, M.H.; Tung, C.P.; Sui, C.H.; Yang, F.H. Estimating seasonal basin rainfall using tabu search. *TAO* **2006**, *17*, 295–316. [CrossRef]
34. Delft Hydraulics. *SOBEK Software User's Manual*; WL | Delft Hydraulics: Delft, The Netherlands, 2013.
35. Risi, R.D.; Paola, F.D.; Turpie, J.; Kroeger, T. Life cycle cost and return on investment as complementary decision variables for urban flood risk management in developing countries. *Int. J. Disaster Risk Reduct.* **2018**, *28*, 88–106. [CrossRef]

36. Chang, H.K.; Tan, Y.C.; Lai, J.S.; Pan, T.Y.; Liu, T.M.; Tung, C.P. Improvement of a drainage system for flood management with assessment of the potential effects of climate change. *Hydrol. Sci. J.* **2013**, *58*, 1581–1597. [CrossRef]
37. Carrivick, J.L. Application of 2D hydrodynamic modelling to high-magnitude outburst floods: An example from Kverkfjöll, Iceland. *J. Hydrol.* **2006**, *321*, 187–199. [CrossRef]
38. Prinsen, G.D.; Becker, B.P.J. Application of sobek hydraulic surface water models in the netherlands hydrological modelling instrument. *Irrig. Drain.* **2011**, *60*, 35–41. [CrossRef]
39. Fan, X.; Tang, C.X.; van Westen, C.J.; Alkema, D. Simulating dam-breach flood scenarios of the Tangjiashan landslide dam induced by the Wenchuan Earthquake. *Nat. Hazards Earth Syst. Sci.* **2012**, *12*, 3031–3044. [CrossRef]
40. Doong, D.J.; Lo, W.; Vojinovic, Z.; Lee, W.L.; Lee, S.P. Development of a new generation of flood inundation maps—A case study of the coastal city of Tainan, Taiwan. *Water* **2016**, *8*, 521. [CrossRef]
41. Yang, S.Y.; Chan, M.H.; Chang, C.H.; Hsu, C.T. A case study of flood risk transfer effect caused by land development in flood-prone lowlands. *Nat. Hazards* **2018**, *91*, 863–878. [CrossRef]
42. Chang, M.J.; Chang, H.K.; Chen, Y.C.; Lin, G.F.; Chen, P.A.; Lai, J.S.; Tan, Y.C. A Support Vector Machine Forecasting Model for Typhoon Flood Inundation Mapping and Early Flood Warning Systems. *Water* **2018**, *10*, 1734. [CrossRef]
43. Poser, K.; Dransch, D. Volunteered geographic information for disaster management with application to rapid flood damage estimation. *Geomatica* **2010**, *64*, 89–98.
44. Hirata, E.; Giannotti, M.A.; Larocca, A.P.C.; Quintanilha, J.A. Flooding and inundation collaborative mapping—Use of the crowdmap/ushahidi platform in the city of Sao Paulo-Brazil. *J. Flood Risk Manag.* **2015**, *11*, 98–109. [CrossRef]
45. Fohringer, J.; Dransch, D.; Kreibich, H.; Schröter, K. Social media as an information source for rapid flood inundation mapping. *Nat. Hazards Earth Syst. Sci.* **2015**, *15*, 2725–2738. [CrossRef]
46. Rosser, J.F.; Leibovici, D.G.; Jackson, M.J. Rapid flood inundation mapping using social media, remote sensing and topographic data. *Nat Hazards* **2017**, *87*, 103–120. [CrossRef]
47. Norbiato, D.; Borga, M.; Degli Esposti, S.; Gaume, E.; Anquetin, S. Flash flood warning based on rainfall thresholds and soil moisture conditions: An assessment for gauged and ungauged basins. *J. Hydrol.* **2008**, *362*, 274–290. [CrossRef]
48. Joo, J.; Lee, J.; Kim, J.H.; Jun, H.; Jo, D. IET definition setting procedure for urban drainage systems. *Water* **2014**, *6*, 45–58. [CrossRef]
49. Yoo, C.; Park, C.; Jun, C. Evaluation of the concept of critical rainfall duration by bivariate frequency analysis of annual maximum independent rainfall event series in Seoul, Korea. *J. Hydrol. Eng.* **2016**, *21*, 1–12. [CrossRef]
50. Cheng, K.S.; Hueter, I.; Hsu, E.C.; Yeh, H.C. A scale-invariant Gauss-Markov model for design storm hyetographs. *J. Am. Water Resour. Assoc.* **2001**, *37*, 723–735. [CrossRef]
51. Vieux, B.E.; Bedient, P.B. Estimation of rainfall for flood prediction from WSR-88D reflectivity: A case study, 17–18 October 1994. *Am. Meteorol. Soc.* **1998**, *13*, 407–415. [CrossRef]
52. Toth, E.; Brath, A.; Montanari, A. Comparison of short-term rainfall prediction models for real-time flood forecasting. *J. Hydrol.* **2000**, *239*, 132–147. [CrossRef]
53. Arnaud, P.; Bouvier, C.; Cisneros, L.; Dominguez, R. Influence of rainfall spatial variability on flood prediction. *J. Hydrol.* **2002**, *260*, 216–230. [CrossRef]
54. Bracken, L.J.; Cox, N.J.; Shannon, J. The relationship between rainfall inputs and flood generation in south–east Spain. *Hydrol. Process.* **2008**, *22*, 683–696. [CrossRef]
55. Montesarchio, V.; Lombardo, F.; Napolitano, F. Rainfall thresholds and flood warning: An operative case study. *Nat. Hazards Earth Syst. Sci.* **2009**, *9*, 135–144. [CrossRef]
56. Golian, S.; Fallahi, M.R.; Behbahani, S.M.; Sharifi, S.; Sharma, A. Real-time updating of rainfall threshold curves for flood forecasting. *J. Hydrol. Eng.* **2014**, *20*, 04014059. [CrossRef]
57. Caporali, E.; Cavigli, E.; Petrucci, A. The index rainfall in the regional frequency analysis of extreme events in Tuscany (Italy). *Environmetrics* **2008**, *19*, 714–724. [CrossRef]
58. Mandal, S.; Choudhury, B.U. Estimation and prediction of maximum daily rainfall at Sagar Island using best fit probability models. *Appl. Clim.* **2015**, *121*, 87–97. [CrossRef]

59. Zheng, C.; Wang, P. Parameter structure identification using tabu search and simulated annealing. *Adv. Water Resour.* **1996**, *19*, 215–224. [CrossRef]
60. Zheng, C.; Wang, P.P. An integrated global and local optimization approach for remediation system design. *Water Resour. Res.* **1999**, *35*, 137–148. [CrossRef]
61. Tung, C.P.; Chou, C.A. Application of tabu search to ground water parameter zonation. *J. Am. Water Resour. Assoc.* **2002**, *38*, 1115–1125. [CrossRef]
62. Leahy, P.; Kiely, G.; Corcoran, G. Structural optimisation and input selection of an artificial neural network for river level prediction. *J. Hydrol.* **2008**, *355*, 192–201. [CrossRef]